Rakenteiden Mekaniikka (Journal of Structural Mechanics)
Vol. 47, No 3, 2014, pp. 110 – 126

A numerical study of the extended finite element method for linear elastic fracture mechanics

Tom Gustafsson[1], Mika Juntunen and Rolf Stenberg

Summary. The extended finite element method combines the flexibility of mesh-independent discontinuities and the accuracy of singular enrichment functions. This paper introduces the method in the context of linear elasticity and gives an overview of its current state of research.

Key words: XFEM, linear elasticity

Received 29 August 2014. Accepted 9 December 2014. Published online 19 December 2014

Introduction

Extended finite element methods (XFEMs) are Galerkin methods where the approximation space is enriched with additional basis functions in order to have an implicit representation of a discontinuity inside the domain and to improve the approximation properties near parts of the domain where singular behavior can be expected. The former implies that the original discretization mesh is not required to conform with a discontinuity—such as a crack in an elastic material. The latter enables the use of uniform discretization in the parts of the domain where a graded mesh would otherwise be recommended, for example, due to reduced rate of convergence caused by sharp corners [26]. These concepts are illustrated in Figure 1.

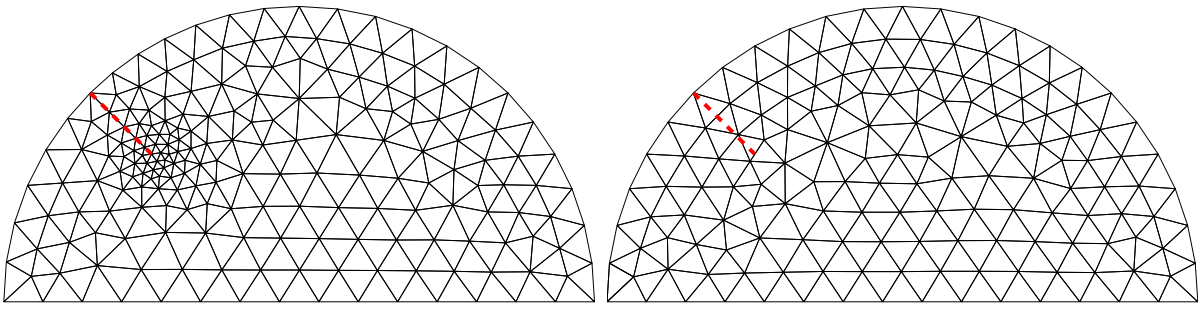

Figure 1. The difference between the meshing strategies in the standard and extended finite element methods. The red dashed line represents a crack in an elastic material. On the left, the elements conform with the crack and the mesh is more refined near the crack tip—as recommended when applying the standard finite element method. On the right, the crack is oriented arbitrarily with respect to the elements and the element size is approximately uniform which is possible when using the extended finite element method.

[1]Corresponding author. tom.gustafsson@aalto.fi

The method and, in particular, its application to fracture mechanical problems is often attributed to Belytschko–Black [6] and Moës et al. [30]. However, its connection to the partition of unity method of Melenk–Babuška [29] is already emphasized in the original article of Belytschko and Black [6]. In fact, extended finite element methods can usually be interpreted in the framework of generalized finite element methods (GFEMs) in sense of Babuška et al. [4]. For more information about the origins of the discussed methods and different naming conventions, see the review papers Fries–Belytschko [18], Babuška et al. [4] and Belytschko et al. [7], the textbooks Pommier et al. [36] and Zhuang et al. [44], or the monographs by Mohammadi [32, 33] and Chahine [10]. A particularly accurate description of the early history of XFEM/GFEM is provided in Babuška–Banerjee [3].

Although a typical application field is fracture mechanics, the extended finite element method has also been applied to areas such as electromagnetism [28] and fluid mechanics [14, 15]. In addition to the simulation of strong discontinuities (such as cracks), procedures exist for taking into account weak discontinuities where a jump in the gradient of the solution is caused by, for example, a discontinuous material parameter, cf. Fries–Belytschko [18]. In this article we consider only linear elastic domains with cracks.

There exist many variants of the extended finite element method [11, 13, 12, 37]. The variants mainly differ in their enrichment strategy, that is, how the additional basis functions are constructed and where they are located. The method we present here is sometimes referred to as the standard XFEM with a fixed enrichment area [27] or XFEM with a geometrical enrichment [5]. This variant is characterized by an enrichment strategy where the mesh nodes inside a fixed radius from the crack tip are enriched locally in addition to the discontinuous enrichment along the crack.

An optimal *a priori* error estimate was reported in Nicaise et al. [35] for the solution of the elasticity equations in two-dimensional polygonal domains using the extended finite element method. The optimality means that an asymptotic convergence rate of order $O(h)$ is obtainable by using piecewise-linear basis functions combined with the XFEM enrichments whereas the standard finite element method with piecewise-linear basis functions would be limited to a convergence rate of order $O(h^{1/2})$ in a similar cracked domain, cf. Braess [9]. In addition, some work in the area of *a posteriori* error estimation exists [19].

The extended finite element method has also been applied to three-dimensional problems [31, 41, 39] although its usefulness is limited by the fact that the crack front asymptotics are not well known for arbitrarily oriented highly curved cracks in three-dimensional domains (see Yosibash [43] for a brief listing of open problems related to the mathematics of fracture mechanics). Therefore, any attempt to enrich the crack front area is unlikely to recover the optimal asymptotic rate of convergence for general three-dimensional domains. A variant of the method with numerically constructed enrichment functions is presented in Duarte–Kim [16] and might provide a solution to this problem.

In this article we formulate the extended finite element method in two-dimensions, present the *a priori* error estimate of Nicaise et al. [35] and verify it numerically. Some remarks are given on the implementation of the extended finite element method. The goal is to familiarize the reader with the method and its current state of research.

The problem statement

We consider two-dimensional polygonal domains $\Omega \subset \mathbb{R}^2$ whose boundaries are characterized by N non-intersecting line segments $\Gamma_k \subset \partial\Omega$, $k \in \{1, \cdots, N\}$, that form a closed path. Thus, if we have N distinct corner points $\boldsymbol{c}_k \in \mathbb{R}^2$, $k \in \{1, \cdots, N\}$, $\boldsymbol{c}_{N+1} = \boldsymbol{c}_1$, we

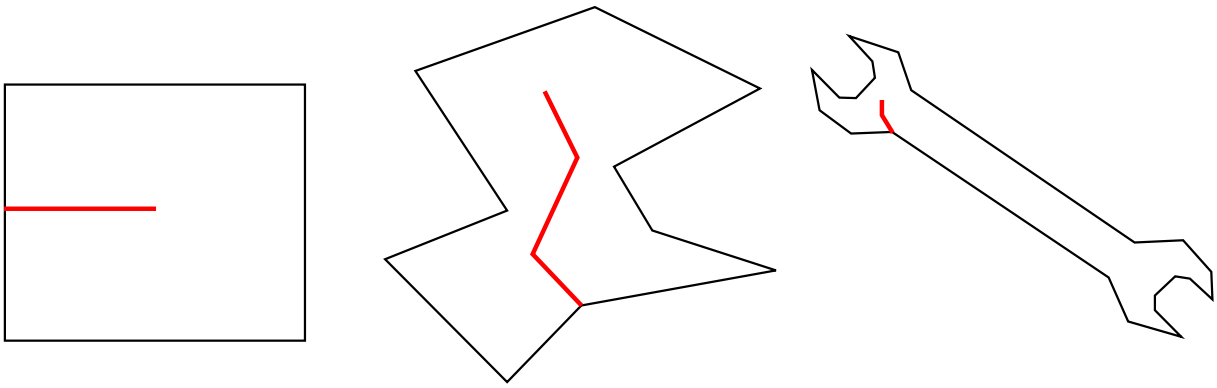

Figure 2. Examples of polygonal domains. The black lines represent the boundary of the uncracked domain Ω and the thicker red lines represent the crack.

may write

$$\Gamma_k = \{t\boldsymbol{c}_k + (1-t)\boldsymbol{c}_{k+1} \,|\, t \in (0,1)\}, \quad k \in \{1, \cdots, N\},$$

and

$$\partial\Omega = \bigcup_{k=1}^{N} \overline{\Gamma_k}, \quad \overline{\Gamma_i} \cap \overline{\Gamma_j} = \begin{cases} \overline{\Gamma_i} = \overline{\Gamma_j} & \text{if } i = j, \\ \{\boldsymbol{c}_j\} & \text{if } (i,j) \in \{(j-1,j),(N,1)\}, \\ \{\boldsymbol{c}_i\} & \text{if } (i,j) \in \{(i,i-1),(1,N)\}, \\ \varnothing & \text{otherwise.} \end{cases}$$

Next we introduce a crack $\Sigma \subset \Omega$ which is also a union of M mutually non-intersecting line segments Σ_k, $k \in \{1, \cdots, M\}$, between the defining points $\boldsymbol{p}_k \in \mathbb{R}^2$, $k \in \{1, \cdots, M+1\}$, such that

$$\Sigma_k = \{t\boldsymbol{p}_k + (1-t)\boldsymbol{p}_{k+1} \,|\, t \in (0,1)\}, \quad \Sigma = \bigcup_{k=1}^{M} \overline{\Sigma_k},$$

with the further requirements that $\partial\Omega \cap \Sigma_k = \varnothing \ \forall k \in \{1, \cdots, M\}$ and $\boldsymbol{p}_k \in \partial\Omega$ if and only if $k = 1$. This implies that the crack Σ intersects the boundary of the domain Ω only at one point $\boldsymbol{p}_1$. Some valid combinations of Ω and Σ are visualized in Figure 2. See also Figure 3 for an example of the introduced notation.

Let $\widetilde{\Omega} = \Omega \setminus \Sigma$ be the cracked domain and $\boldsymbol{n} \in \mathbb{R}^2$ be an unit outward normal to $\partial\widetilde{\Omega}$. Furthermore, let $\Gamma_N, \Gamma_D \subset \partial\Omega$ be non-empty parts of the boundary with prescribed traction and homogeneous displacement, respectively. The computational domain is $\widetilde{\Omega}$ in which we seek for a displacement field $\boldsymbol{u} : \widetilde{\Omega} \to \mathbb{R}^2$ satisfying

$$\begin{aligned} -\nabla \cdot \boldsymbol{\sigma}(\boldsymbol{u}) &= \boldsymbol{f} \quad \text{in } \widetilde{\Omega}, \\ \boldsymbol{\sigma}(\boldsymbol{u})\boldsymbol{n} &= \boldsymbol{g} \quad \text{on } \Gamma_N, \\ \boldsymbol{\sigma}(\boldsymbol{u})\boldsymbol{n} &= \boldsymbol{0} \quad \text{on } \Sigma, \\ \boldsymbol{u} &= \boldsymbol{0} \quad \text{on } \Gamma_D, \end{aligned} \tag{1}$$

for a given body load $\boldsymbol{f} \in [L^2(\widetilde{\Omega})]^2$ and traction $\boldsymbol{g} \in [H^{1/2}(\Gamma_N)]^2$. For the definition of the function spaces L^2 and H^k, $k > 0$, see for example Adams [2]. In addition to the equations in (1), we have the stress-strain and strain-displacement relationships

$$\boldsymbol{\sigma}(\boldsymbol{u}) = 2\mu\left[\boldsymbol{\epsilon}(\boldsymbol{u}) + (\lambda + 2\mu)^{-1}\lambda \operatorname{tr}\boldsymbol{\epsilon}(\boldsymbol{u})\boldsymbol{I}\right], \tag{2}$$

$$\boldsymbol{\epsilon}(\boldsymbol{u}) = \frac{1}{2}\left(\nabla\boldsymbol{u} + \nabla\boldsymbol{u}^T\right), \tag{3}$$

where μ and λ are the Lamé parameters and $\boldsymbol{I}$ is an identity tensor. Note that (2) is valid only for the plane stress configuration where the modeled object is assumed to be thin in the third dimension.

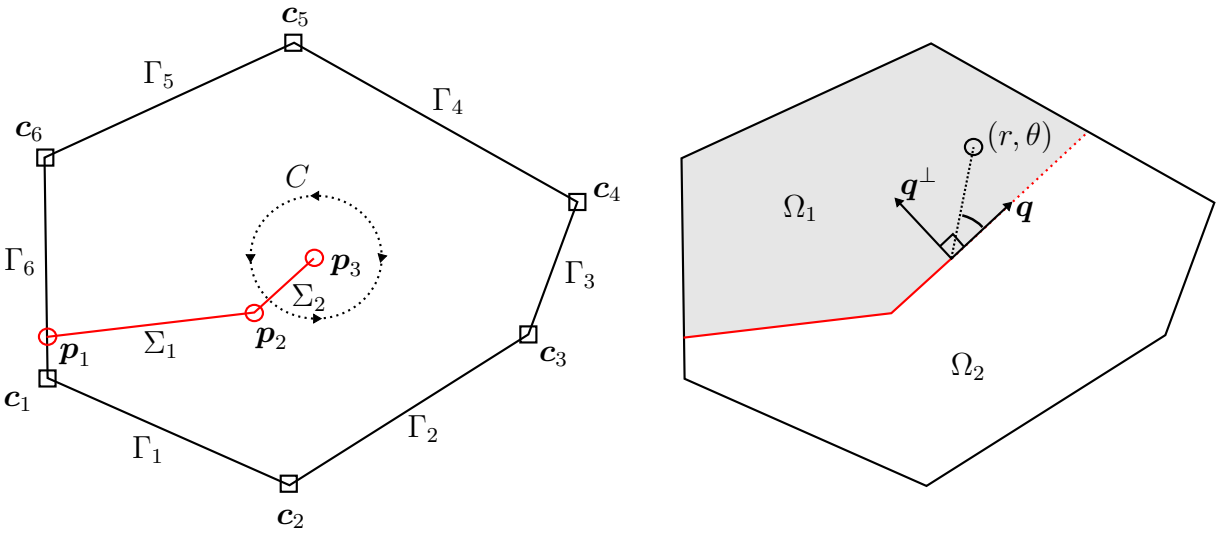

Figure 3. The naming conventions used in the paper.

The equations in (1) together with the relationships (2) and (3) form the equations of linear elasticity [34]. The equations of linear elasticity have been applied to model brittle fracture ever since the pioneering works of Griffith [20], Westergaard [42] and Irwin [24]. Nevertheless, the main unknown of the equations, the displacement field, might not be the most interesting engineering variable with regard to fracture development. A more comprehensive view can be given by the so-called stress intensity factors K_I and K_{II} that are computed through the following functionals of $\boldsymbol{u}$ [38]: Suppose that $\boldsymbol{f} = \boldsymbol{0}$ and let $\boldsymbol{q} = (\boldsymbol{p}_{M+1} - \boldsymbol{p}_M)\|\boldsymbol{p}_{M+1} - \boldsymbol{p}_M\|^{-1}$ be the crack extension direction. Then

$$K_I(\boldsymbol{u}) = \int_C \boldsymbol{\sigma}(\boldsymbol{u}) : \boldsymbol{\epsilon}(\boldsymbol{u}_I)(\boldsymbol{n}\cdot\boldsymbol{q}) - \boldsymbol{\sigma}(\boldsymbol{u})\boldsymbol{n}\cdot(\nabla\boldsymbol{u}_I)\boldsymbol{q} - \boldsymbol{\sigma}(\boldsymbol{u}_I)\boldsymbol{n}\cdot(\nabla\boldsymbol{u})\boldsymbol{q}\,\mathrm{d}s, \tag{4}$$

$$K_{II}(\boldsymbol{u}) = \int_C \boldsymbol{\sigma}(\boldsymbol{u}) : \boldsymbol{\epsilon}(\boldsymbol{u}_{II})(\boldsymbol{n}\cdot\boldsymbol{q}) - \boldsymbol{\sigma}(\boldsymbol{u})\boldsymbol{n}\cdot(\nabla\boldsymbol{u}_{II})\boldsymbol{q} - \boldsymbol{\sigma}(\boldsymbol{u}_{II})\boldsymbol{n}\cdot(\nabla\boldsymbol{u})\boldsymbol{q}\,\mathrm{d}s, \tag{5}$$

where C is a counterclockwise path around the crack tip such that its endpoints lie on the line segment Σ_M and $\boldsymbol{n}$ is an outward unit normal vector to the path. Furthermore, the asymptotic displacements $\boldsymbol{u}_I$ and $\boldsymbol{u}_{II}$ are defined using the crack tip polar coordinate system (r,θ) originated at $\boldsymbol{p}_{M+1}$ and oriented by the two orthonormal vectors $\boldsymbol{q} = (q_1, q_2)^T$ and $\boldsymbol{q}^\perp = (-q_2, q_1)^T$ representing the local x- and y-axes, respectively. See Figure 3 for a visual description of the used polar coordinate system. The expressions for $\boldsymbol{u}_I$ and $\boldsymbol{u}_{II}$ are

$$\boldsymbol{u}_I(r,\theta) = \frac{1}{2\mu}\sqrt{\frac{r}{2\pi}}\begin{pmatrix}\cos\frac{\theta}{2}(\delta - \cos\theta)\\ \sin\frac{\theta}{2}(\delta - \cos\theta)\end{pmatrix}, \tag{6}$$

$$\boldsymbol{u}_{II}(r,\theta) = \frac{1}{2\mu}\sqrt{\frac{r}{2\pi}}\begin{pmatrix}\sin\frac{\theta}{2}(2 + \delta + \cos\theta)\\ \cos\frac{\theta}{2}(2 - \delta - \cos\theta)\end{pmatrix}, \tag{7}$$

with $\delta = 3 - \frac{4\lambda}{3\lambda+2\mu}$ under the plane stress conditions. For more information about the prescribed fracture mechanical concepts such as the stress intensity factors see, for ex-

ample, the textbooks by Janssen et al. [25], Yosibash [43] and Grisvard [21]—listed in an increasing order of mathematical content.

As usual for finite element methods, the numerical solution of (1) together with (2) and (3) is done through a weak formulation of the problem. Let $\boldsymbol{V} = \{\boldsymbol{w} \in [H^1(\widetilde{\Omega})]^2 \,\big|\, \boldsymbol{w}|_{\Gamma_D} = \boldsymbol{0}\}$. For the equations of linear elasticity, the weak formulation reads: find a function $\boldsymbol{u} \in \boldsymbol{V}$ that satisfies

$$\int_{\widetilde{\Omega}} \boldsymbol{\sigma}(\boldsymbol{u}) : \boldsymbol{\epsilon}(\boldsymbol{v}) \,\mathrm{d}x = \int_{\Gamma_N} \boldsymbol{g} \cdot \boldsymbol{v} \,\mathrm{d}s + \int_{\widetilde{\Omega}} \boldsymbol{f} \cdot \boldsymbol{v} \,\mathrm{d}x, \tag{8}$$

for every test function $\boldsymbol{v} \in \boldsymbol{V}$.

Discretization

In the extended finite element method, additional basis functions are included in the discrete finite element space in order to improve its approximation properties. Additional accuracy might be required, for example, near points where the domain has corners or crack tips. It is well known that near such features the solution of (8) is not properly approximated by polynomial functions [40]. Thus, the added functions should represent the local behavior of the solution as closely as possible.

When additional basis functions are added into the discrete space, we say that the discrete space is *enriched* and the added functions are called *enrichments*. The particular enrichments used in the XFEM for fracture problems are inspired by the fact that the crack tip stress field is always asymptotically a linear combination of the stresses corresponding to the displacements (6) and (7) while approaching the crack tip in two-dimensional plane stress media [21].

In addition to an accurate crack tip approximation, the discontinuity caused by the crack can be represented independent of the mesh by enriching the discrete space with certain discontinuous basis functions. This allows us to use a single computational mesh with various different crack configurations and, therefore, reduce the overall effort in the meshing process.

The enrichment procedure is performed in such a way that we start with a collection of piecewise-linear basis functions—the so-called hat functions—attached to the nodes of the mesh. For some subset of hat functions we apply a modification operation and the resulting set of modified basis functions is augmented to the basis which spans the discrete space. In order to formulate the enrichment procedure, we need to define the node sets for which the corresponding hat functions are modified.

Suppose that we have a triangulation $\mathcal{T}_h = \{K\}$ of the uncracked domain Ω where h refers to the mesh parameter and $\overline{\Omega} = \cup_{K \in \mathcal{T}_h} \overline{K}$. This means that the elements are not required to conform with the crack, that is, $K \cap \Sigma$ is not necessarily an empty set. However, we make the simplifying assumption that the crack Σ does not go through any vertices of the mesh and that no element is intersected twice by the crack. These are simply technical difficulties that can be overcome either through local mesh modifications or by duplication of nodes. Multiply-cracked elements can be handled by adding multiple enrichments to the nodes of the corresponding elements [8].

Let us denote with $\boldsymbol{\mathcal{N}}_j$, $j \in \mathcal{N} = \{1, \cdots, N_{\text{nodes}}\}$, the nodes of the mesh $\mathcal{T}_h$ where N_{nodes} is the total amount of nodes in the mesh. The subset of nodes which are included in the crack tip enrichment, denoted by $\mathscr{X}$, are chosen to be the nodes which are inside

a certain fixed radius $\mathcal{R}$ of the crack tip $\boldsymbol{p}_{M+1}$. Thus,

$$\mathscr{X} = \left\{ j \in \mathscr{N} \,\middle|\, \|\boldsymbol{\mathcal{N}}_j - \boldsymbol{p}_{M+1}\| \leq \mathcal{R} \right\}. \tag{9}$$

Furthermore, the subset of nodes which are included in the discontinuous enrichment, denoted by $\mathscr{J}$, are chosen to be the nodes for which the neighboring elements do not contain the crack tip but at least some of them are nevertheless intersected by the crack. Hence, if $\operatorname{neigh}(\boldsymbol{\mathcal{N}}_j) = \{K \in \mathcal{T}_h \,|\, \boldsymbol{\mathcal{N}}_j \in \overline{K}\}$ are the elements that have $\boldsymbol{\mathcal{N}}_j$ as a vertex then

$$\mathscr{J} = \left\{ j \in \mathscr{N} \,\middle|\, \operatorname{neigh}(\boldsymbol{\mathcal{N}}_j) \cap \Sigma \neq \varnothing \text{ and } \boldsymbol{p}_{M+1} \notin \operatorname{neigh}(\boldsymbol{\mathcal{N}}_j) \right\}. \tag{10}$$

The nodes belonging to the sets $\mathscr{X}$ and $\mathscr{J}$ are illustrated in Figure 4.

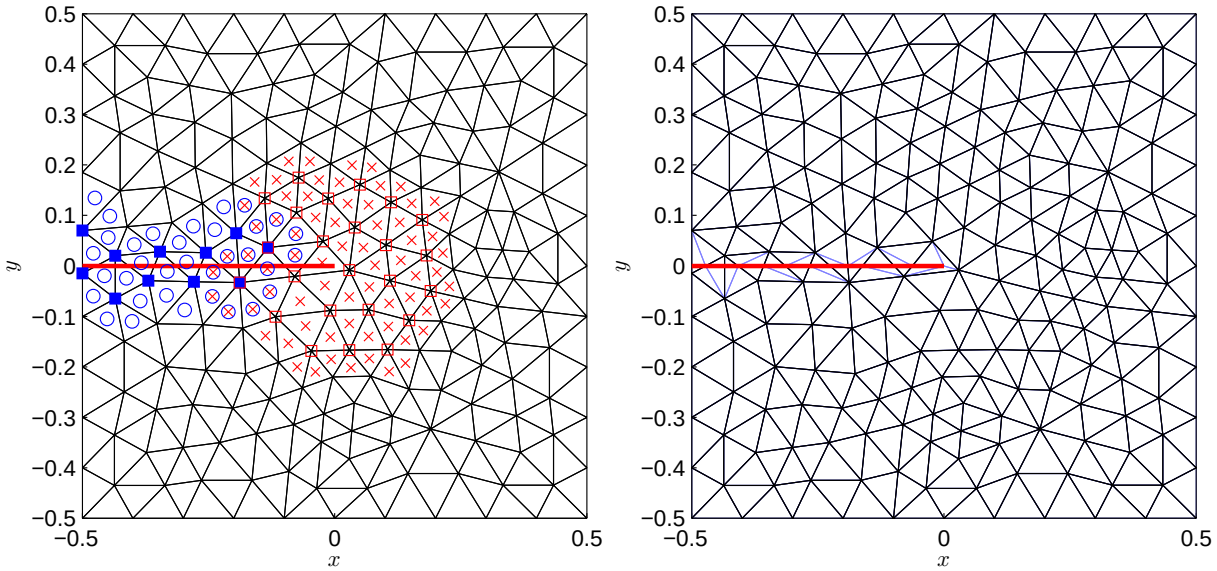

Figure 4. An example domain and a mesh. On the left, the nodes with a discontinuous enrichment belonging to $\mathscr{J}$ are denoted by blue solid squares whereas the nodes with a crack tip enrichment belonging to $\mathscr{X}$ are denoted by red hollow squares (here $\mathcal{R} = 0.2$). The elements in which numerical integration must be performed due to the added basis functions are denoted by blue disks and red crosses, respectively. The thick red line corresponds to the crack. On the right, the elements that are intersected by the crack are split into subtriangles in order to construct accurate integration rules.

Let $\mathscr{N}_D$ be the indices of the nodes at the Dirichlet boundary Γ_D. The standard piecewise-linear basis functions φ_j, $j \in \mathscr{N} \setminus \mathscr{N}_D$, are defined such that they are linear in each element $K \in \mathcal{T}_h$ and satisfy $\varphi_j(\boldsymbol{\mathcal{N}}_j) = \delta_{ij}$ for all $i, j \in \mathscr{N} \setminus \mathscr{N}_D$ where δ_{ij} is the Kronecker delta symbol. The following notation is used to build up the basis for the approximation of the extended finite element method. Let f be an arbitrary function and A be a subset of $\mathscr{N}$. Then we define

$$\mathcal{B}_A(f) = \left\{ \begin{pmatrix} f\varphi_j \\ 0 \end{pmatrix} \,\middle|\, j \in A \setminus \mathscr{N}_D \right\} \cup \left\{ \begin{pmatrix} 0 \\ f\varphi_j \end{pmatrix} \,\middle|\, j \in A \setminus \mathscr{N}_D \right\}. \tag{11}$$

Through the crack and its straight extension (see Figure 3), the domain can be split into two parts Ω_1 and Ω_2. Using the functions

$$H(\boldsymbol{x}) = \begin{cases} 1 & \text{if } \boldsymbol{x} \in \Omega_1, \\ -1 & \text{if } \boldsymbol{x} \in \Omega_2, \end{cases} \tag{12}$$

$$\tag{13}$$

$$\widetilde{F}_1(\boldsymbol{x}) = F_1(r,\theta) = \sqrt{r}\sin\frac{\theta}{2}, \tag{14}$$

$$\widetilde{F}_2(\boldsymbol{x}) = F_2(r,\theta) = \sqrt{r}\cos\frac{\theta}{2}, \tag{15}$$

$$\widetilde{F}_3(\boldsymbol{x}) = F_3(r,\theta) = \sqrt{r}\sin\frac{\theta}{2}\sin\theta, \tag{16}$$

$$\widetilde{F}_4(\boldsymbol{x}) = F_4(r,\theta) = \sqrt{r}\cos\frac{\theta}{2}\sin\theta, \tag{17}$$

the discrete space of the extended finite element method is written as

$$\boldsymbol{V}_h = \operatorname{span}\left[\mathcal{B}_{\mathscr{N}}(1) \cup \mathcal{B}_{\mathscr{J}}(H) \cup \bigcup_{i=1}^{4} \mathcal{B}_{\mathscr{X}}(\widetilde{F}_i)\right] \subset \boldsymbol{V}. \tag{18}$$

Finally, the discrete formulation reads: find $\boldsymbol{u}_h \in \boldsymbol{V}_h$ such that

$$\int_{\widetilde{\Omega}} \boldsymbol{\sigma}(\boldsymbol{u}_h) : \boldsymbol{\epsilon}(\boldsymbol{v}_h)\,\mathrm{d}x = \int_{\Gamma_N} \boldsymbol{g}\cdot\boldsymbol{v}_h\,\mathrm{d}s + \int_{\widetilde{\Omega}} \boldsymbol{f}\cdot\boldsymbol{v}_h\,\mathrm{d}x, \tag{19}$$

is satisfied for every $\boldsymbol{v}_h \in \boldsymbol{V}_h$. The solution of (19) will obey the following *a priori* error esimate proven originally by Nicaise et al. [35]. For a more careful review of the proof see a recent Master's thesis by Gustafsson [23]. To formulate the upcoming theorem, we use the usual H^1 and H^2 norms defined by

$$\|w\|_{1,D}^2 = \int_D w^2\,\mathrm{d}x + \int_D \nabla w\cdot\nabla w\,\mathrm{d}x$$

and

$$\|w\|_{2,D}^2 = \|w\|_{1,D}^2 + \int_D \left(\frac{\partial^2 w}{\partial x^2}\right)^2 + 2\left(\frac{\partial^2 w}{\partial x\partial y}\right)^2 + \left(\frac{\partial^2 w}{\partial y^2}\right)^2 \mathrm{d}x.$$

For vector-valued functions we interpret

$$\|\boldsymbol{w}\|_{k,D}^2 = \|w_1\|_{k,D}^2 + \|w_2\|_{k,D}^2.$$

Theorem 1. *Let $\chi : [0,\infty) \to [0,1]$ be a sufficiently smooth cutoff function satisfying*

$$\begin{cases} \chi(r) = 1 & \text{if } r < \frac{\mathcal{R}}{2}, \\ 0 < \chi(r) < 1 & \text{if } \frac{\mathcal{R}}{2} < r < \mathcal{R}, \\ \chi(r) = 0 & \text{if } r > \mathcal{R}. \end{cases}$$

Assume that the solution $\boldsymbol{u} \in [H^1(\widetilde{\Omega})]^2$ to the continuous problem (8) satisfies

$$\boldsymbol{u} - \chi(r)(K_I(\boldsymbol{u})\boldsymbol{u}_I + K_{II}(\boldsymbol{u})\boldsymbol{u}_{II})) = \boldsymbol{u} - \chi(r)\boldsymbol{u}_S \in [H^2(\widetilde{\Omega})]^2.$$

Then for the discrete solution $\boldsymbol{u}_h$ of (19) we have the estimate

$$\|\boldsymbol{u} - \boldsymbol{u}_h\|_{1,\widetilde{\Omega}} \leq Ch\left(\|\boldsymbol{u} - \chi(r)\boldsymbol{u}_S\|_{2,\widetilde{\Omega}} + \|\boldsymbol{u}_S\|_{1,\widetilde{\Omega}}\right).$$

Implementation issues

The implementation of the extended finite element method differs slightly from the implementation of the standard finite element method. In order to integrate exactly on both sides of the crack, a subtriangulation which follows the crack must be computed. Fortunately, this subtriangulation is not required to satisfy any shape regularity constraints as it is used only to generate quadrature points. See Figure 4 for an example subtriangulation and Figure 5 for the distribution of quadrature points near the discontinuity for the same mesh.

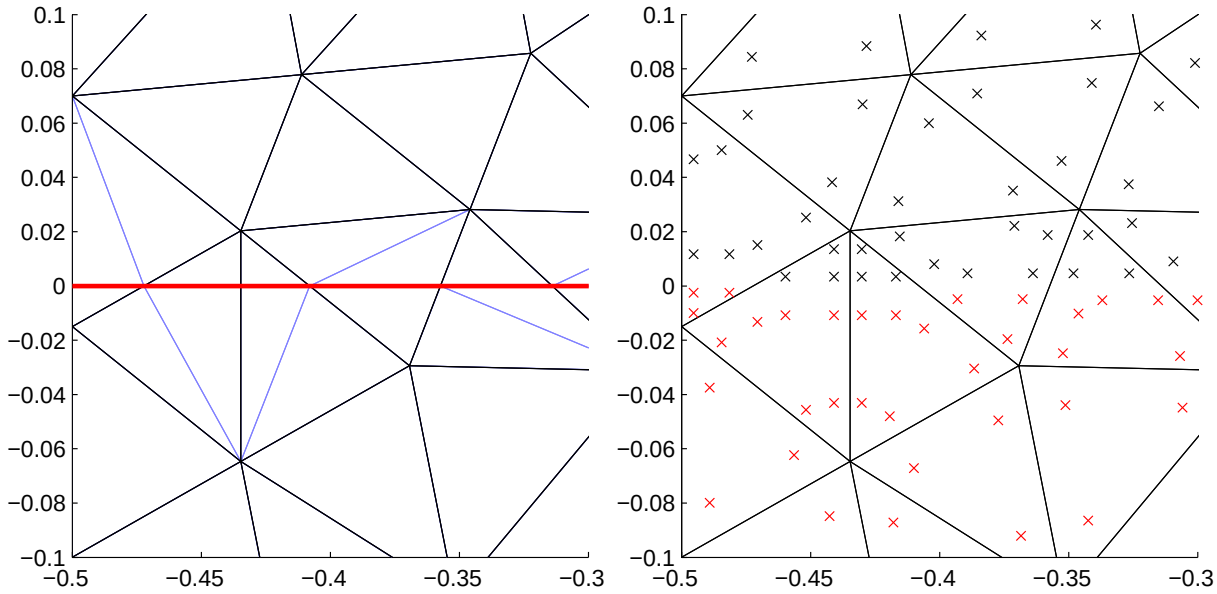

Figure 5. On the left, a zoomed view of Figure 4. On the right, the distribution of second-order exact Dunavant quadrature points through the subtriangulation. Color indicates the sign of $H(\boldsymbol{x})$ as defined in (12).

Although finding such a subtriangulation is straightforward in two-dimensions, the internal representation of the discontinuity should be flexible enough for a convenient manipulation of the crack location. The usage of level-sets to define the location of a discontinuity has showed its potential and also extends to three-dimensional problems [36, p. 29]. In our in-house code and this paper we have chosen a conceptually simpler approach of defining the crack explicitly as a set of line segments.

Additional care must be taken when integrating the non-polynomial terms caused by the non-polynomial crack tip basis functions, for example, in $\mathcal{B}_{\mathscr{X}}(\widetilde{F}_1)$. An exact quadrature rule is not known to exist although special quadrature rules have been developed, for example, in Laborde et al. [27] that perform better than any standard rules with respect to the number of quadrature points. In our code we employ the so-called Dunavant quadrature points [17] even though they are not specifically tailored for the presence of the crack tip singularity. The effect of inaccurate integration is studied in the numerical experiments.

The inclusion of additional basis functions will increase the size of the resulting stiffness matrix. If the degrees of freedom are numbered such that the first N_{nodes} degrees of freedom correspond to the x-displacements and the rest to the y-displacements, the

resulting symmetric stiffness matrix $\boldsymbol{K}$ can be written as the block matrix

$$\boldsymbol{K} = \begin{bmatrix} \boldsymbol{K}_{xx} & \boldsymbol{K}_{xy} \\ \boldsymbol{K}_{xy}^T & \boldsymbol{K}_{yy} \end{bmatrix}, \tag{20}$$

where

$$(\boldsymbol{K}_{xx})_{ij} = \int_{\widetilde{\Omega}} \boldsymbol{\sigma}(\begin{pmatrix} \phi_j \\ 0 \end{pmatrix}) : \boldsymbol{\epsilon}(\begin{pmatrix} \phi_i \\ 0 \end{pmatrix}) \,\mathrm{d}x, \tag{21}$$

$$(\boldsymbol{K}_{xy})_{ij} = \int_{\widetilde{\Omega}} \boldsymbol{\sigma}(\begin{pmatrix} 0 \\ \phi_j \end{pmatrix}) : \boldsymbol{\epsilon}(\begin{pmatrix} \phi_i \\ 0 \end{pmatrix}) \,\mathrm{d}x, \tag{22}$$

$$(\boldsymbol{K}_{yy})_{ij} = \int_{\widetilde{\Omega}} \boldsymbol{\sigma}(\begin{pmatrix} 0 \\ \phi_j \end{pmatrix}) : \boldsymbol{\epsilon}(\begin{pmatrix} 0 \\ \phi_i \end{pmatrix}) \,\mathrm{d}x, \tag{23}$$

and

$$\phi_i = \begin{cases} \varphi_i & \text{if } i \in \mathscr{N}, \\ H\varphi_i & \text{if } i \in \{|\mathscr{N}|+1, \cdots, |\mathscr{N}|+|\mathscr{J}|\}, \\ \widetilde{F}_k\varphi_i & \text{if } i \in \{|\mathscr{N}|+|\mathscr{J}|+(k-1)|\mathscr{X}|+1, \cdots, |\mathscr{N}|+|\mathscr{J}|+k|\mathscr{X}|\}. \end{cases} \tag{24}$$

Furthermore, every submatrix $\boldsymbol{K}_{xx}$, $\boldsymbol{K}_{xy}$ and $\boldsymbol{K}_{yy}$ can be split into nine submatrices by the different types of basis functions in (24). For example,

$$\boldsymbol{K}_{xx} = \begin{bmatrix} \boldsymbol{A} & \boldsymbol{B} & \boldsymbol{C} \\ \boldsymbol{B}^T & \boldsymbol{D} & \boldsymbol{E} \\ \boldsymbol{C}^T & \boldsymbol{E}^T & \boldsymbol{F} \end{bmatrix}, \tag{25}$$

where

$$(\boldsymbol{A})_{ij} = \int_{\widetilde{\Omega}} \boldsymbol{\sigma}(\begin{pmatrix} \varphi_j \\ 0 \end{pmatrix}) : \boldsymbol{\epsilon}(\begin{pmatrix} \varphi_i \\ 0 \end{pmatrix}) \,\mathrm{d}x \qquad i,j \in \mathscr{N},$$

$$(\boldsymbol{B})_{ij} = \int_{\widetilde{\Omega}} \boldsymbol{\sigma}(\begin{pmatrix} H\varphi_j \\ 0 \end{pmatrix}) : \boldsymbol{\epsilon}(\begin{pmatrix} \varphi_i \\ 0 \end{pmatrix}) \,\mathrm{d}x \qquad i \in \mathscr{N}, j \in \{1, \cdots, |\mathscr{J}|\},$$

$$(\boldsymbol{C})_{ij} = \int_{\widetilde{\Omega}} \boldsymbol{\sigma}(\begin{pmatrix} \widetilde{F}_k\varphi_j \\ 0 \end{pmatrix}) : \boldsymbol{\epsilon}(\begin{pmatrix} \varphi_i \\ 0 \end{pmatrix}) \,\mathrm{d}x \qquad i \in \mathscr{N}, j \in \{(k-1)|\mathscr{X}|+1, \cdots, k|\mathscr{X}|\},$$
$$k \in \{1,2,3,4\},$$

$$(\boldsymbol{D})_{ij} = \int_{\widetilde{\Omega}} \boldsymbol{\sigma}(\begin{pmatrix} \widetilde{F}_k\varphi_j \\ 0 \end{pmatrix}) : \boldsymbol{\epsilon}(\begin{pmatrix} H\varphi_i \\ 0 \end{pmatrix}) \,\mathrm{d}x \qquad i \in \{1, \cdots, |\mathscr{J}|\},$$
$$j \in \{(k-1)|\mathscr{X}|+1, \cdots, k|\mathscr{X}|\},$$
$$k \in \{1,2,3,4\},$$

$$(\boldsymbol{E})_{ij} = \int_{\widetilde{\Omega}} \boldsymbol{\sigma}(\begin{pmatrix} \widetilde{F}_k\varphi_j \\ 0 \end{pmatrix}) : \boldsymbol{\epsilon}(\begin{pmatrix} \widetilde{F}_k\varphi_i \\ 0 \end{pmatrix}) \,\mathrm{d}x \qquad i,j \in \{(k-1)|\mathscr{X}|+1, \cdots, k|\mathscr{X}|\},$$
$$k \in \{1,2,3,4\}.$$

The other submatrices of $\boldsymbol{K}$ can be split similarly. The sparsity pattern of the resulting stiffness matrix for the configuration of Figure 4 is visualized in Figure 6.

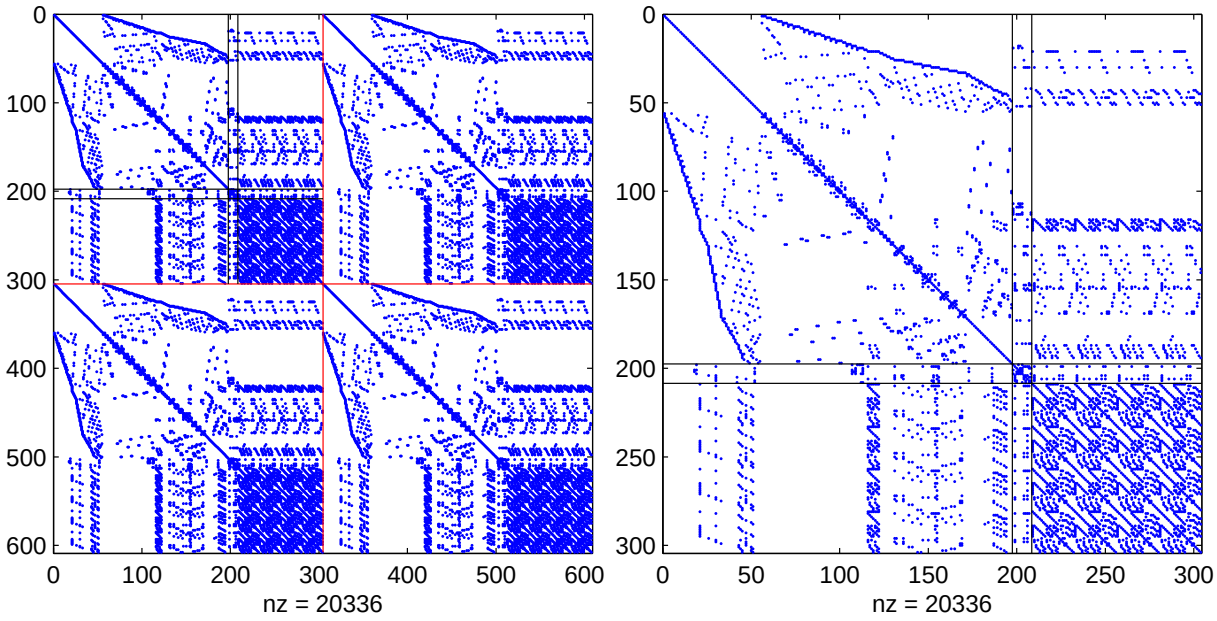

Figure 6. The sparsity pattern of the stiffness matrix. On the left, the non-zeros of the whole system matrix $\boldsymbol{K}$ are highlighted. The red vertical and horizontal lines in the middle separate the blocks $\boldsymbol{K}_{xx}, \boldsymbol{K}_{xy}, \boldsymbol{K}_{xy}^T$ and $\boldsymbol{K}_{yy}$. On the right, a closer view of the upper-left submatrix $\boldsymbol{K}_{xx}$. The lines again separate the blocks of $\boldsymbol{K}_{xx}$ as defined in (25). The domain and the mesh are the same as in Figure 4.

The sparsity pattern of Figure 6 reveals that the lower-right corner of the submatrix $\boldsymbol{K}_{xx}$ of (25), equating to $\boldsymbol{F}$, has a high fill-in. This is due to the fact that multiple basis functions have exactly the same support inside the crack tip radius. The discontinuous basis functions are only limited to the nodes of the triangles cut by the crack and hence the size of the matrix $\boldsymbol{D}$ is small. Moreover, the size of the matrix $\boldsymbol{F}$ is heavily dependent on the enrichment radius $\mathcal{R}$. For large values of $\mathcal{R}$ or small values of h, the size of $\boldsymbol{F}$ might even surpass the size of the matrix $\boldsymbol{A}$ which corresponds to the stiffness matrix of the standard finite element method. This means that the computational time spent solving the final linear system of equations is higher than for the standard finite element method.

Implementation of the method into an existing two-dimensional finite element code turned out to be fairly straightforward although special care must be taken in order to efficiently implement the additional data structures and the subtriangulation routine. Note that in three spatial dimensions the work becomes much more involved, cf. Sukumar et al. [41].

Numerical experiments

In order to verify the estimate of Theorem 1 we consider a problem setting similar to the one in Figure 4. An exact solution is known if the whole outer boundary (that is, excluding the crack boundaries) is set to a Dirichlet condition with values equal to some superposition of $\boldsymbol{u}_I$ and $\boldsymbol{u}_{II}$ that both satisfy the traction-free condition at the crack boundaries and also satisfy the equilibrium equation with $\boldsymbol{f} = \boldsymbol{0}$. We choose the boundary values to be equal to $10^9\,\boldsymbol{u}_I + 10^8\,\boldsymbol{u}_{II}$ and the material parameters $E = 210\,\mathrm{GPa}$ with $\nu = 0.3$. Furthermore, we consider only plane stress conditions. The enrichment radius was chosen to be $\mathcal{R} = 0.2$ and a tenth-order Dunavant quadrature rule was used

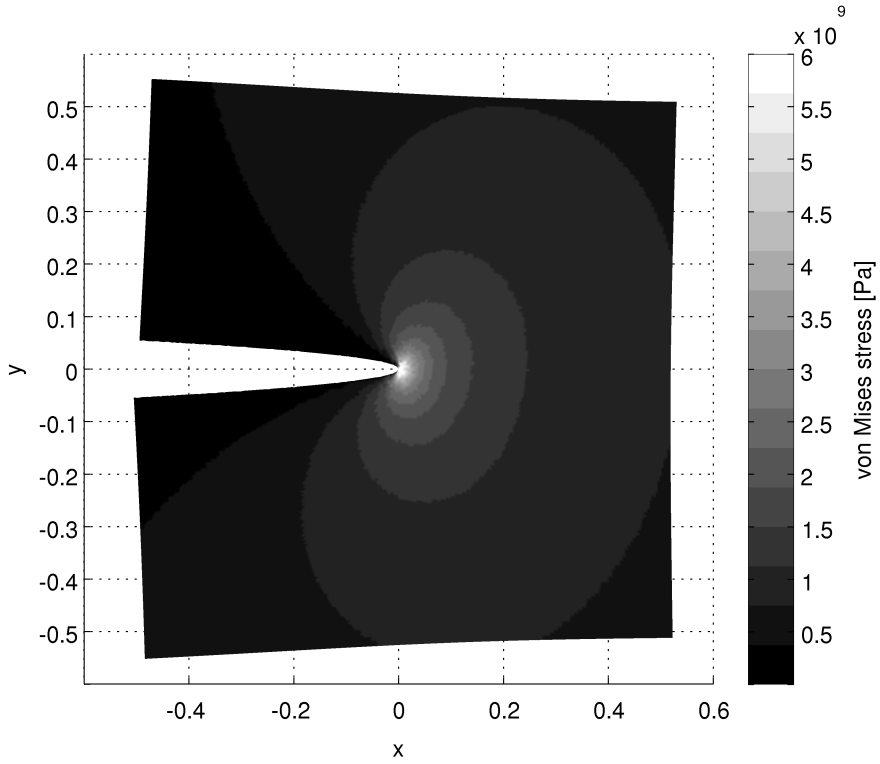

Figure 7. The von Mises stress and the displaced geometry (scaling factor equals to 10) with 90112 elements in the original mesh and $h = 0.0075$. White color represents stresses higher than $6 \cdot 10^9$ Pa.

in the elements inside the enrichment radius. A second-order quadrature rule was used in the other elements.

The resulting displacement field and post-processed von Mises stress are visualized in Figure 7. The convergence rate of the finite element solution in H^1 norm is shown in Figure 8. The linear fittings to the numerical data in Figure 8 verify the statement of Theorem 1 and show that a suboptimal (with respect to the polynomial order) convergence rate of order $O(h^{1/2})$ is obtained when using the standard finite element method and that a higher order of convergence can be obtained with the extended finite element method.

One severe downside of the discussed XFEM variant is that the condition number of the system matrix $\boldsymbol{K}$ will increase approximately as $O(h^8)$ while for standard finite element method it increases only as $O(h^2)$. This is demonstrated numerically in Figure 9. An intuitive reason behind this is that the added basis functions can be fairly similar to the already included standard hat functions, for example, when $r \approx \mathcal{R}$ and large enrichment radii are used. This significantly reduces the usefulness of iterative solvers and will ultimately induce numerical error even with direct solvers. An improvement in the conditioning issue of the stiffness matrix has been reported in Gupta et al. [22] and was achieved by modifying the set of additional crack tip basis functions such that they are maximally orthogonal to the standard piecewise-linear basis functions.

In order to demonstrate the necessity of an accurate quadrature rule, we compared the H^1 error of the solution when integrating with various orders of Dunavant rule in the crack tip triangles. The results are visualized in Figure 10 and show that the H^1 error might stagnate rapidly when using too low-order integration rules. Thus, even though no exact integration rules exist it should always be verified that the incorporated quadrature is exact enough for the desired numerical accuracy.

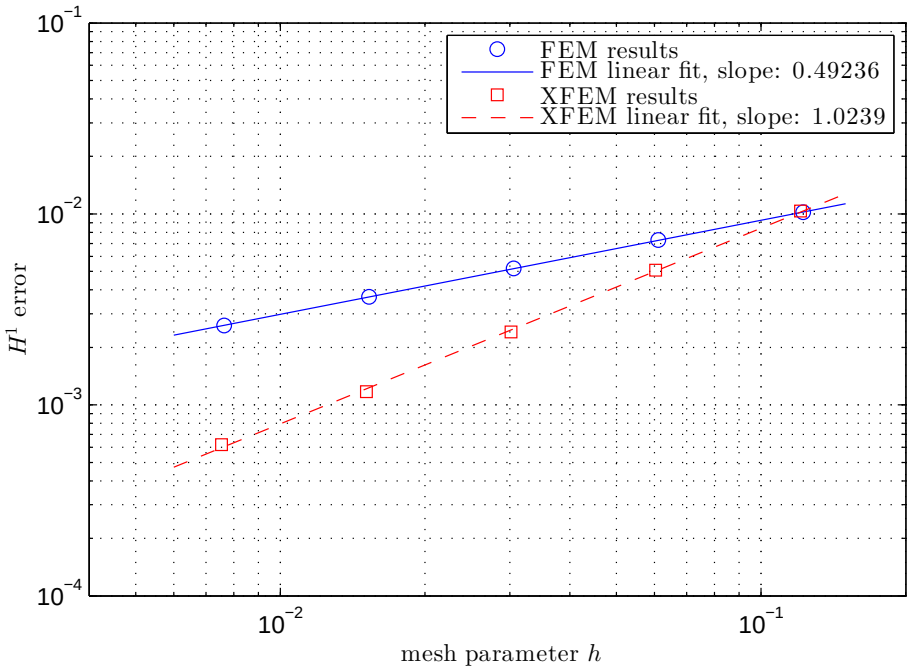

Figure 8. The convergence rate of H^1 error $\|\boldsymbol{u} - \boldsymbol{u}_h\|_{1,\widetilde{\Omega}}$ with respect to the mesh parameter h. Here $\mathcal{R} = 0.2$ and a tenth-order Dunavant quadrature was used in the crack tip triangles.

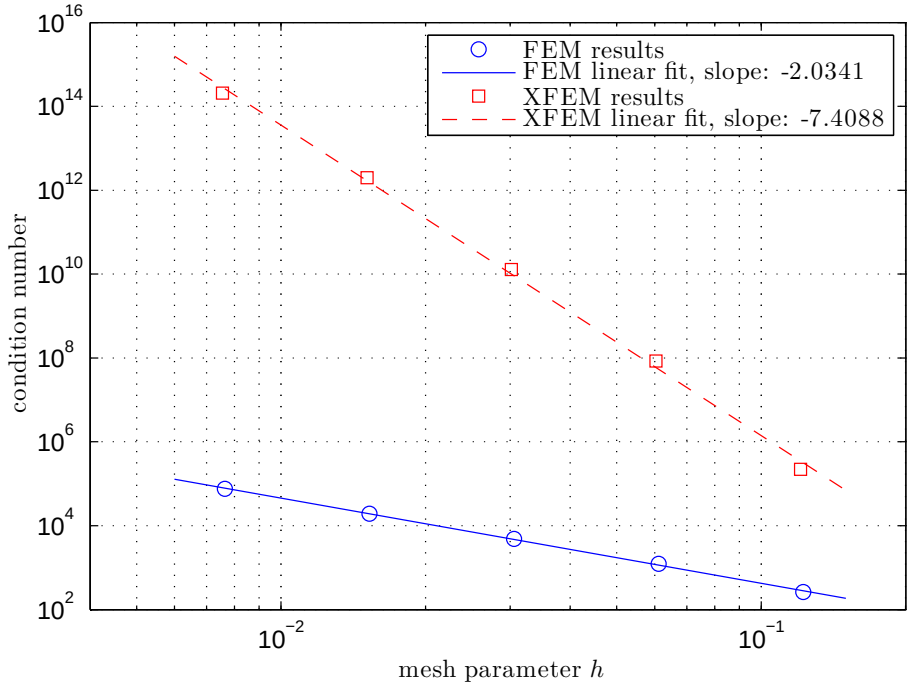

Figure 9. The condition number of the system matrix $\boldsymbol{K}$ as estimated by the MATLAB command *condest* for the standard and extended finite element methods.

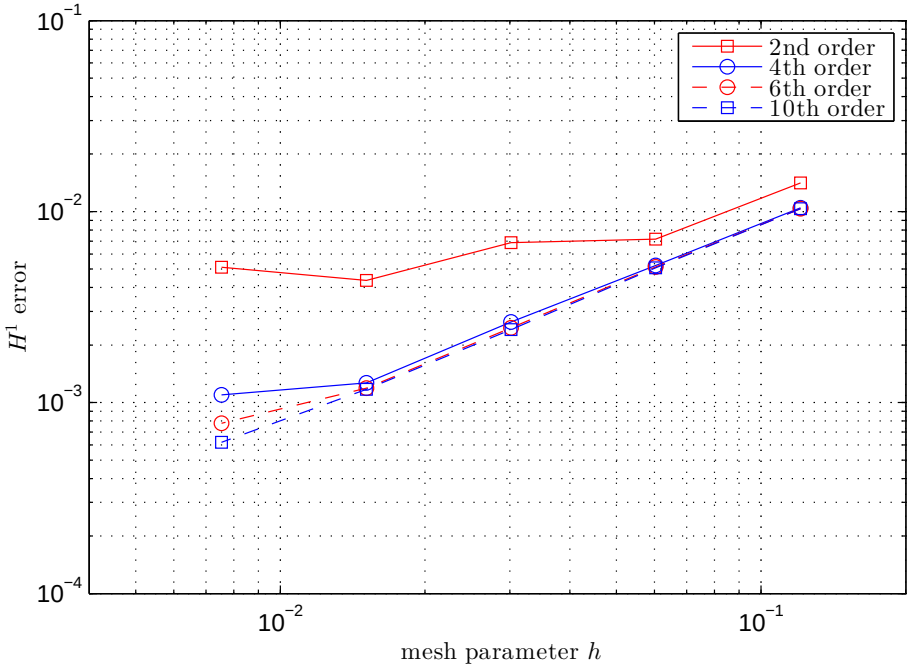

Figure 10. The effect of varying the order of the crack tip Dunavant quadrature rule to the H^1 error. The H^1 error is always evaluated using a tenth-order quadrature. Here the enrichment radius is $\mathcal{R} = 0.1$.

The inclusion of additional and properly chosen basis functions has been shown to increase the rate of convergence of the finite element solution. This is, in fact, something that has been known for decades: Strang–Fix [40] already proposed the inclusion of the crack tip functions in 1973 for the solution of the Poisson equation. The essential contribution of the extended finite element method is the combination of the crack tip enrichments and the clever representation of the discontinuity in order to obtain a flexible method to experiment with different crack configurations and even perform crack propagation studies. The concept of a flexible discontinuity representation is demonstrated in Figure 11 by solving the elasticity equations in a single domain with the same initial mesh, boundary conditions and two different crack locations.

Concluding remarks

A two-dimensional extended finite element method for fracture mechanics was presented and numerically verified to provide better convergence rates in H^1 norm than the standard finite element method with piecewise-linear elements. The method was demonstrated to provide a flexible way to experiment with various crack configurations and therefore it can also be a viable choice for crack propagation studies where the location of the discontinuity is constantly evolving.

Although the lack of three-dimensional asymptotic results for arbitrarily curved cracks reduces the usefulness of the extended finite element method for three-dimensional modeling [23], its merits related to the flexibility of the crack location are obviously recognized amongst the commercial finite element community. For example, the three-dimensional extended finite element support in Abaqus of Dassault Systèmes is constantly updated—most recently in the version 6.14 of the software package released in 2014 [1]. This suggests that the commercial interest in mesh-independent crack simulation studies is not decreasing.

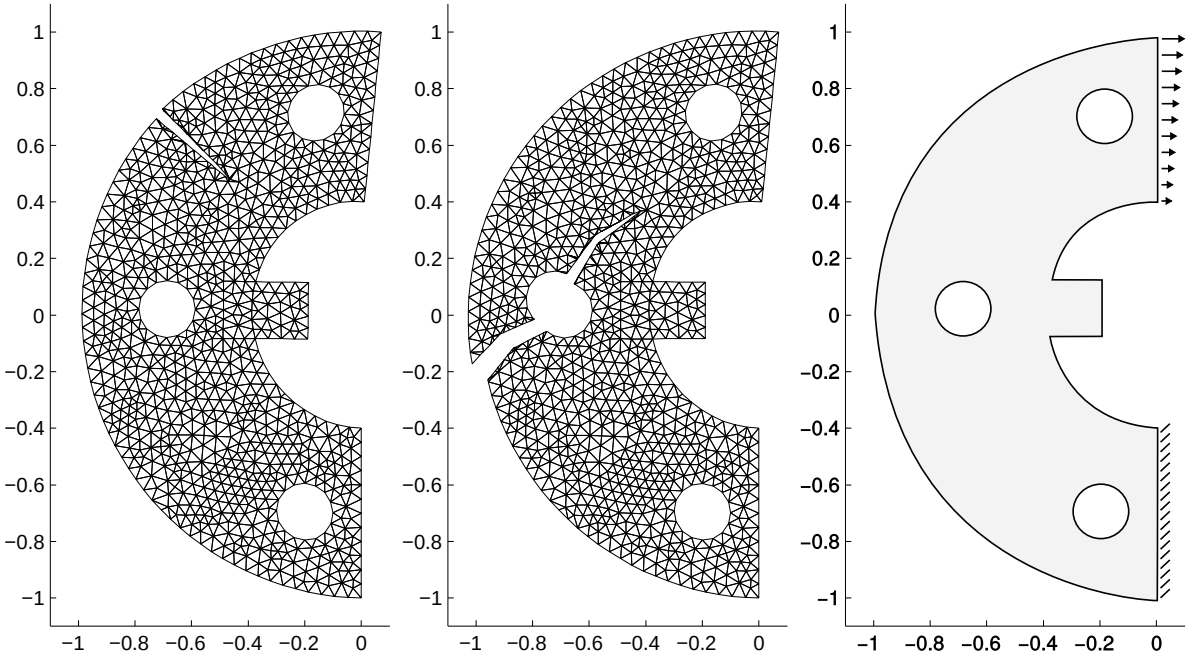

Figure 11. Same initial mesh with two different crack configurations. The mesh is deformed according to the solved displacement. Material constants are the same as in the previous convergence study. Upper-right corner of the object is displaced slightly while the lower-right corner is fixed. The traction on the upper-right boundary is defined such that the solution satisfies $\boldsymbol{u}(x, y) = (\frac{1}{10}(y - \frac{3}{10}), 0)^T$ on the respective boundary.

Acknowledgements

Financial support from Tekes—the Finnish Funding Agency for Innovation—is gratefully acknowledged (Decision nr. 40205/12).

References

[1] What's new in Abaqus 6.14. [Online; accessed on August 2014]. http://www.3ds.com/products-services/simulia/portfolio/abaqus/latest-release/.

[2] R. A. Adams and J. J. Fournier. *Sobolev Spaces, 2nd Edition*. Academic Press, 2003. ISBN 9780120441433.

[3] I. Babuška and U. Banerjee. Stable Generalized Finite Element Method (SGFEM). *Computer Methods in Applied Mechanics and Engineering*, 201–204, 2012. doi:10.1016/j.cma.2011.09.012.

[4] I. Babuška, U. Banerjee, and J. E. Osborn. Survey of meshless and generalized finite element methods: A unified approach. *Acta Numerica*, 12:1–125, 2003. doi:10.1017/S0962492902000090.

[5] E. Béchet, H. Minnebo, N. Moës, and B. Burgardt. Improved implementation and robustness study of the X-FEM for stress analysis around cracks. *International Journal for Numerical Methods in Engineering*, 64:1033–1056, 2005. doi:10.1002/nme.1386.

[6] T. Belytschko and T. Black. Elastic crack growth in finite elements with minimal remeshing. *International Journal for Numerical Methods in Engineering*, 45(5):601–620, 1999. doi:10.1002/(SICI)1097-0207(19990620)45:5<601::AID-NME598>3.0.CO;2-S.

[7] T. Belytschko, R. Gracie, and G. Ventura. A review of extended/generalized finite element methods for material modelling. *Modelling and Simulation in Materials Science and Engineering*, 17, 2009. doi:10.1088/0965-0393/17/4/043001.

[8] S. Bordas, P. V. Nguyen, C. Dunant, A. Guidoum, and H. Nguyen-Dang. An extended finite element library. *International Journal for Numerical Methods in Engineering*, 71(6): 703–732, 2007. doi:10.1002/nme.1966.

[9] D. Braess. *Finite Elements: Theory, fast solvers, and applications in solid mechanics. Second edition.* Cambridge University Press, 2001. doi:10.1017/CBO9780511618635.

[10] E. Chahine. *Etude Mathématique et Numérique de Méthodes d'Éléments Finis Étendues Pour Le Calcul en Domaines Fissurés.* PhD thesis, Institut National des Sciences Appliquées de Toulouse, 2005. Published also by VDM Verlag Dr. Müller under the title *eXtended Finite Element Method (XFEM): Mathematical and Numerical Study for Cracked Domains Computations.*

[11] E. Chahine, P. Laborde, and Y. Renard. Crack tip enrichment in the XFEM using a cutoff function. *International Journal for Numerical Methods in Engineering*, 75(6):629–646, 2008. doi:10.1002/nme.2265.

[12] E. Chahine, P. Laborde, and Y. Renard. A non-conformal eXtended Finite Element Approach: Integral matching XFEM. *Applied Numerical Mathematics*, 61(3):322–343, 2011. doi:10.1016/j.apnum.2010.10.009.

[13] E. Chahine, P. Laborde, and Y. Renard. Spider XFEM, an extended finite element variant for partially unknown crack-tip displacement. *European Journal of Computational Mechanics*, 17(5–7):625–636, 2012. doi:10.3166/remn.17.625-636.

[14] J. Chessa and T. Belytschko. An extended finite element method for two-phase fluids. *Journal of Applied Mechanics*, 70:10–17, 2003. doi:10.1115/1.1526599.

[15] Y. J. Choi, M. A. Hulsen, and Meijer H. E. H. An extended finite element method for the simulation of particulate viscoelastic flows. *Journal of Non-Newtonian Fluid Mechanics*, 165:607–624, 2010. doi:10.1016/j.jnnfm.2010.02.021.

[16] C. A. Duarte and D. J. Kim. Analysis and applications of a generalized finite element method with global-local enrichment functions. *Computer Methods in Applied Mechanics and Engineering*, 197(6–8):487–504, 2008. doi:10.1016/j.cma.2007.08.017.

[17] D. A. Dunavant. High degree efficient symmetrical Gaussian quadrature rules for the triangle. *International Journal for Numerical Methods in Engineering*, 21(6):1129–1148, 1985. doi:10.1002/nme.1620210612.

[18] T.P. Fries and T. Belytschko. The extended/generalized finite element method: An overview of the method and its applications. *International Journal for Numerical Methods in Engineering*, 84(3):253–304, 2010. doi:10.1002/nme.2914.

[19] T. Gerasimov, M. Rüter, and E. Stein. An explicit residual-type error estimator for Q1-quadrilateral extended finite element method in two-dimensional linear elastic fracture mechanics. *International Journal for Numerical Methods in Engineering*, 90(9):1118–1155, 2012. doi:10.1002/nme.3363.

[20] A. A. Griffith. The Phenomena of Rupture and Flow in Solids. *Philosophical Transactions of the Royal Society of London*, 211:163–196, 1920.

[21] P. Grisvard. *Singularities in Boundary Value Problems*. Masson, 1992. ISBN 2-225-82770-2.

[22] V. Gupta, C. A. Duarte, I. Babuška, and U. Banerjee. A stable and optimally convergence generalized FEM (SGFEM) for linear elastic fracture mechanics. *Computational Methods in Applied Mechanical Engineering*, 266:23–39, 2013. doi:10.1016/j.cma.2013.07.010.

[23] T. Gustafsson. Extended finite element method for computing stress intensity factors. Master's thesis, Aalto University School of Science, 2014.

[24] G. R. Irwin. Analysis of Stresses and Strains Near the End of a Crack Traversing a Plate. *Journal of Applied Mechanics*, 24:361–364, 1957.

[25] M. Janssen, J. Zuidema, and R. Wanhill. *Fracture Mechanics, 2nd Edition*. Spon Press, 2004. ISBN 0-415-34622-3.

[26] P. Laasonen. On the degree of convergence of discrete approximations for the solutions of the Dirichlet problem. *Annales Academiæ Scientiarum Fennicæ. Series A I.*, (246), 1957.

[27] P. Laborde, J. Pommier, Y. Renard, and M. Salaun. High-order extended finite element method for cracked domains. *International Journal for Numerical Methods in Engineering*, 64:354–381, 2005. doi:10.1002/nme.1370.

[28] F. Lefèvre, S. Lohrengel, and S. Nicaise. An extended finite element method for 2D edge elements. *International journal of numerical analysis and modeling*, 8(4):641–666, 2011.

[29] J. M. Melenk and I. Babuška. The partition of unity finite element method: basic theory and applications. *Computer Methods in Applied Mechanics and Engineering*, 39:289–314, 1996. doi:10.1016/S0045-7825(96)01087-0.

[30] N. Moës, J. Dolbow, and T. Belytschko. A finite element method for crack growth without remeshing. *International Journal for Numerical Methods in Engineering*, 46(1):131–150, 1999. doi:10.1002/(SICI)1097-0207(19990910)46:1<131::AID-NME726>3.0.CO;2-J.

[31] N. Moës, A. Gravouil, and T. Belytschko. Non-planar 3D crack growth by the extended finite element and level sets—Part I: Mechanical model. *International Journal for Numerical Methods in Engineering*, 53:2549–2568, 2002. doi:10.1002/nme.429.

[32] S. Mohammadi. *Extended Finite Element Method for Fracture Analysis of Structures*. Blackwell Publishing Ltd, 2008. doi:10.1002/9780470697795.

[33] S. Mohammadi. *XFEM Fracture Analysis of Composites*. John Wiley & Sons, Ltd., 2012. doi:10.1002/9781118443378.

[34] J. Nečas and I. Hlaváček. *Mathematical Theory of Elastic and Elasto-Plastic Bodies: An Introduction*. Elsevier, 1981. doi:10.1016/B978-0-444-99754-8.50002-3.

[35] S. Nicaise, Y. Renard, and E. Chahine. Optimal convergence analysis for the extended finite element method. *International Journal for Numerical Methods in Engineering*, 86 (4–5):528–548, 2011. doi:10.1002/nme.3092.

[36] S. Pommier, A. Gravouil, A. Combescure, and N. Moës. *Extended Finite Element Method for Crack Propagation*. John Wiley & Sons, Ltd., 2011. doi:10.1002/9781118622650.

[37] J. Réthore, S. Roux, and F. Hild. Hybrid analytical and extended finite element method (HAX-FEM): A new enrichment procedure for cracked solids. *International Journal for Numerical Methods in Engineering*, 81(3):269–285, 2010. doi:10.1002/nme.2691.

[38] J. R. Rice. A Path Independent Integral and the Approximate Analysis of Strain Concentration by Notches and Cracks. *Journal of Applied Mechanics*, 35(2):379–386, 1968.

[39] J. X. Shi, D. Chopp, J. Lua, N. Sukumar, and T. Belytschko. Abaqus implementation of extended finite element using a level set representation for three-dimensional fatigue crack growth and life predictions. *Engineering Fracture Mechanics*, 77(14):2840–2863, 2010. doi:10.1016/j.engfracmech.2010.06.009.

[40] G. Strang and G. J. Fix. *An Analysis of the Finite Element Method*. Prentice Hall, 1973. ISBN 9780130329462.

[41] N. Sukumar, N. Moes, B. Moran, and T. Belytschko. Extended finite element method for three-dimensional crack modelling. *International Journal for Numerical Methods in Engineering*, 48:1549–1570, 2000. doi:10.1002/1097-0207(20000820)48:11<1549::AID-NME955>3.0.CO;2-A.

[42] H. M. Westergaard. Stresses At A Crack, Size Of The Crack, And The Bending Of Reinforced Concrete. *Proceedings of the American Concrete Institute*, 30:93–102, 1933.

[43] Z. Yosibash. *Singularities in Elliptic Boundary Value Problems and Elasticity and Their Connection with Failure Initiation*. Springer, 2012. doi:10.1007/978-1-4614-1508-4.

[44] Z. Zhuang, Z. Liu, B. Cheng, and J. Liao. *Extended Finite Element Method*. Tsinghua University Press, Elsevier Inc, 2014. doi:10.1016/B978-0-12-407717-1.01001-3.

Tom Gustafsson, Mika Juntunen, Rolf Stenberg
Aalto University School of Science, Department of Mathematics and Systems Analysis
P.O. Box 11100, FI-00076 Aalto, Finland
tom.gustafsson@aalto.fi, mojuntun@gmail.com, rolf.stenberg@aalto.fi